

Spring 2016

Measurements of photon beam intensity at the High Intensity Gamma-Ray Source (HIGS) facility for astrophysically relevant photodisintegration reaction cross section

Evan G. Meekins
James Madison University

Follow this and additional works at: <https://commons.lib.jmu.edu/honors201019>

 Part of the [Nuclear Commons](#)

Recommended Citation

Meekins, Evan G., "Measurements of photon beam intensity at the High Intensity Gamma-Ray Source (HIGS) facility for astrophysically relevant photodisintegration reaction cross section" (2016). *Senior Honors Projects, 2010-current*. 214.
<https://commons.lib.jmu.edu/honors201019/214>

This Thesis is brought to you for free and open access by the Honors College at JMU Scholarly Commons. It has been accepted for inclusion in Senior Honors Projects, 2010-current by an authorized administrator of JMU Scholarly Commons. For more information, please contact dc_admin@jmu.edu.

Measurements of Photon Beam Intensity at the High Intensity Gamma-Ray Source (HIγS)
Facility for Astrophysically Relevant Photodisintegration Reaction Cross Section


An Honors Program Project Presented to
the Faculty of the Undergraduate
College of Science and Mathematics
James Madison University


by Evan George Meekins


May 2016

Accepted by the faculty of the Department of Physics and Astronomy, James Madison University, in partial fulfillment of the requirements for the Honors Program.

FACULTY COMMITTEE:

 4/5/2016
Project Advisor: Dr. Adriana Banu, Ph.D.,
Assistant Professor, Department of Physics and
Astronomy

 4/7/2016
Reader: Dr. Keigo Fukumura, Ph.D.,
Assistant Professor, Department of Physics and
Astronomy

 4/7/16
Reader: Dr. Ioana Niculescu, Ph.D.,
Professor, Department of Physics and Astronomy

HONORS PROGRAM APPROVAL:

Bradley R. Newcomer, Ph.D.,
Director, Honors Program

PUBLIC PRESENTATION

This work is accepted for presentation, in part or in full, at Madison Union Ballroom, JMU on April 15th, 2016.

Contents

Figures & Tables.....	3
Acknowledgements.....	4
Abstract.....	5
1 Motivation.....	6
1.1 p-Nuclei.....	8
1.2 $^{94}\text{Mo}(\gamma,n)^{93}\text{Mo}$ Cross Section.....	12
2 Experimental Method.....	14
2.1 HIγS Facility.....	14
2.1.1 Free Electron Laser Beam Production.....	14
2.2 Experimental Setup.....	18
2.2.1 Aluminum Collimator.....	19
2.2.2 ^3He Proportional Counter Array.....	20
2.2.3 HPGe Detector.....	21
2.2.4 Flux Determination Equipment.....	21
3 HIγS Photon Beam Intensity Determination.....	22
3.1 Photoactivation Method.....	23
3.1.1 Photon Beam Intensity Results.....	31
3.1.2 Error Analysis.....	32
3.2 Deuterium Photodisintegration Method.....	34
4 Outlook.....	36
5 References.....	37

Figures & Tables

Figure 1 – s-process visualization.....	6
Figure 2 – r-process visualization.....	7
Figure 3 – Chart of nuclides.....	8
Figure 4 – Limitations of neutron capture processes.....	8
Figure 5 – Isotopic abundances.....	9
Figure 6 – γ -process flow.....	10
Figure 7 – Travaglio simulation results.....	11
Figure 8 – Photodisintegration of nucleus.....	12
Figure 9 – HI γ S Free Electron Laser Facility.....	15
Figure 10 – Undulator System.....	16
Figure 11 – γ -Ray Production.....	17
Figure 12 – Compton back-scattering event.....	17
Figure 13 – Target room setup.....	18
Figure 14 – Collimated HI γ S beam.....	20
Figure 15 – ^3He proportional counter array detector.....	20
Figure 16 – $^{197}\text{Au}(\gamma, n)^{196}\text{Au}$ cross section.....	23
Figure 17 – Decay Scheme of ^{196}Au	24
Figure 18 – 356 keV photopeak summation.....	26
Figure 19 – 356 keV photopeak Gaussian fit.....	27
Figure 20 – Decay of ^{196}Au with time.....	28
Figure 21 – Mixed source HPGe spectrum.....	29
Figure 22 – HPGe calibrations.....	30
Figure 23 – Photon beam intensity determination.....	31
Figure 24 – $^2\text{H}(\gamma, n)$ cross section.....	34
Figure 25 – $(\text{C}_6\text{D}_6)/\text{LSD}$ setup.....	35
Table 1 – p -Nuclei abundances.....	9
Table 2 – Parameterization for $^{197}\text{Au}(\gamma, n)$ cross section.....	27
Table 3 – Mixed source sheet.....	29
Table 4 – HPGe calibration results.....	30
Table 5 – Photon beam intensity determination.....	31
Table 6 – HPGe calibration error.....	33

Acknowledgements

Thank you to the following members of the H γ S collaboration that assisted us in this experiment: Professor Hugon Karwowski (University of North Carolina at Chapel Hill/TUNL), Jack Silano (PhD student, UNC at Chapel Hill), Dr. William Zimmerman (postdoc, TUNL), Professor Werner Tornow (Duke University/TUNL), Dr. Megha Bhike (postdoc, TUNL).

Thank you to the Research Corporation for Science Advancement for funding this experiment.

Thank you to the Department of Physics and Astronomy for continuous support.

Most of all, many thanks to Dr. Adriana Banu, who made all of this and so much more possible.

Abstract

How nuclear reactions in stars and stellar explosions such as supernovae have forged the elements out of hydrogen and helium leftover from the Big Bang is a longstanding, still timely research topic in nuclear astrophysics. Although there is a fairly complete understanding of the production of the chemical elements and their isotopes up to iron by nuclear fusion in stars, important details concerning the production of the elements from iron to uranium remain puzzling. Current knowledge is that the nucleosynthesis beyond iron proceeds mainly via neutron capture reactions and subsequent electron decays to stability. However, some 35 proton-rich stable isotopes, between ^{74}Se and ^{196}Hg , cannot be synthesized by neutron-capture processes, since they are located on the neutron-deficient side of the region of stable isotopes. These proton-rich nuclides are generally referred to as *p*-Nuclei. Among them, ^{94}Mo is the most abundant. Our interest is to constrain the origin of *p*-Nuclei through nuclear physics by studying the cross section of $^{94}\text{Mo}(\gamma, n)^{93}\text{Mo}$, a key photodisintegration reaction for the nucleosynthesis of *p*-Nuclei occurring in Type Ia supernovae. An experiment measuring this reaction cross section was performed at the High Intensity Gamma-Ray Source (HIγS) Facility in the spring of 2014. A crucial role in measuring the $^{94}\text{Mo}(\gamma, n)^{93}\text{Mo}$ cross section is the determination of the photon intensity. In this thesis the two experimental methods that were employed for the photon intensity determination are presented: photoactivation of ^{197}Au and photodisintegration of deuterium. The photon flux was determined range from $(6 - 18) \times 10^7 \pm 5\%$ photons per second.

Chapter 1

Motivation

How nuclear reactions in astrophysical environments forge the chemical elements from the hydrogen and helium left over from the Big Bang is a longstanding, yet still timely research topic in the field of nuclear astrophysics. While there is a fairly complete understanding of the production of the elements up to iron in stars, details important to the synthesis of heavier elements beyond iron remain puzzling and incomplete. Such details are pertinent to models which attempt to replicate the birth and chemical makeup of our own solar system, a goal long sought after by theoretical astrophysicists.

Analogous to how elements up to iron are synthesized in stars by fusing two lighter nuclei together, current knowledge regarding the synthesis of heavy isotopes beyond iron is that neutron capture (n, γ)* reactions play the main role. If this process occurs in a stellar environment with a moderate neutron flux where the probability of neutron capture is low, then it is referred to as slow neutron capture (s-process), as seen in **Figure 1**.

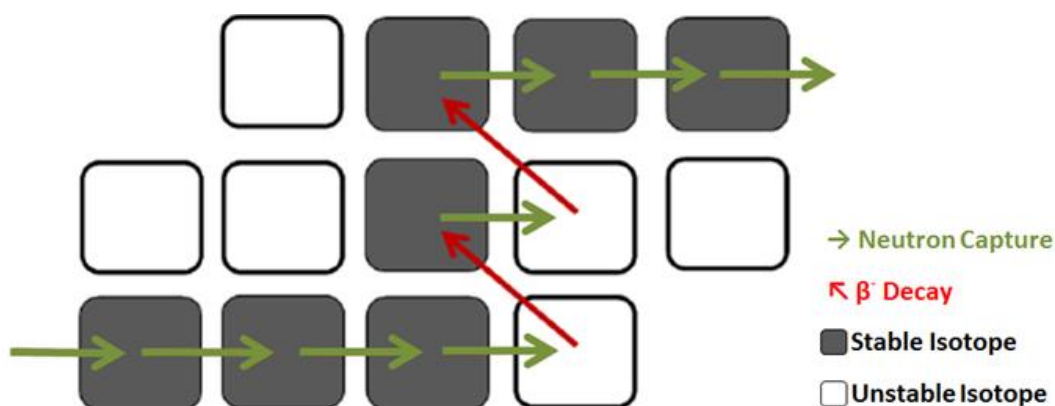


Figure 1: Illustration of the path of the s-process. In a β^- decay a neutron rich unstable nucleus decays into stability by emitting an electron (β^- particle) and an anti-electron neutrino.

* ${}^A_ZX + n \rightarrow {}^{A+1}_ZX + \gamma$

Conversely, in a stellar environment with a high flux of neutrons such that the probability of neutron capture is very high, this process is referred to as rapid neutron capture (r-process), as seen in **Figure 2**.

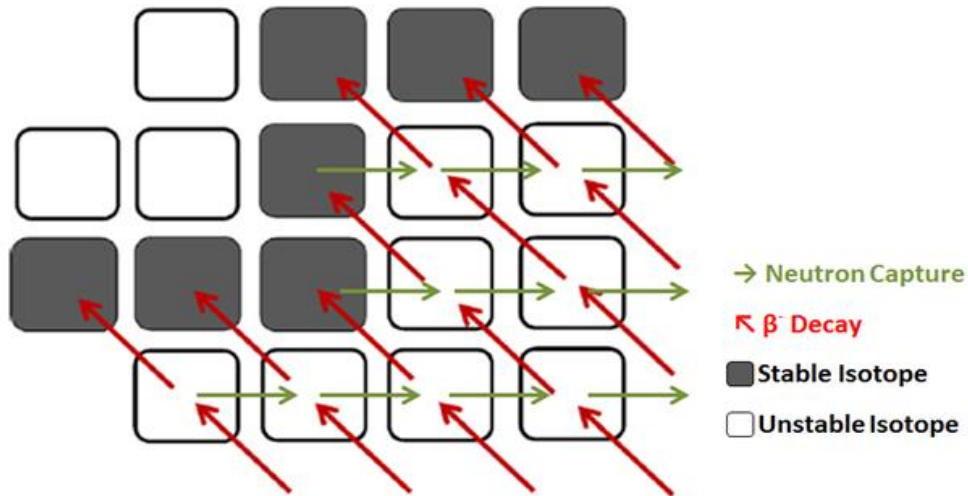


Figure 2: Illustration of the path of the r-process.

While the slow and rapid neutron capture processes provide an answer as to how heavy, neutron rich isotopes can be formed, these reactions cannot contribute to the nucleosynthesis of proton rich heavy isotopes [1].

1.1 *p*-Nuclei

In nature, there are 35 stable proton rich nuclei between ^{74}Se and ^{196}Hg , referred to as *p*-Nuclei and shown in **Figure 3**, which are the rarest of all stable nuclei.

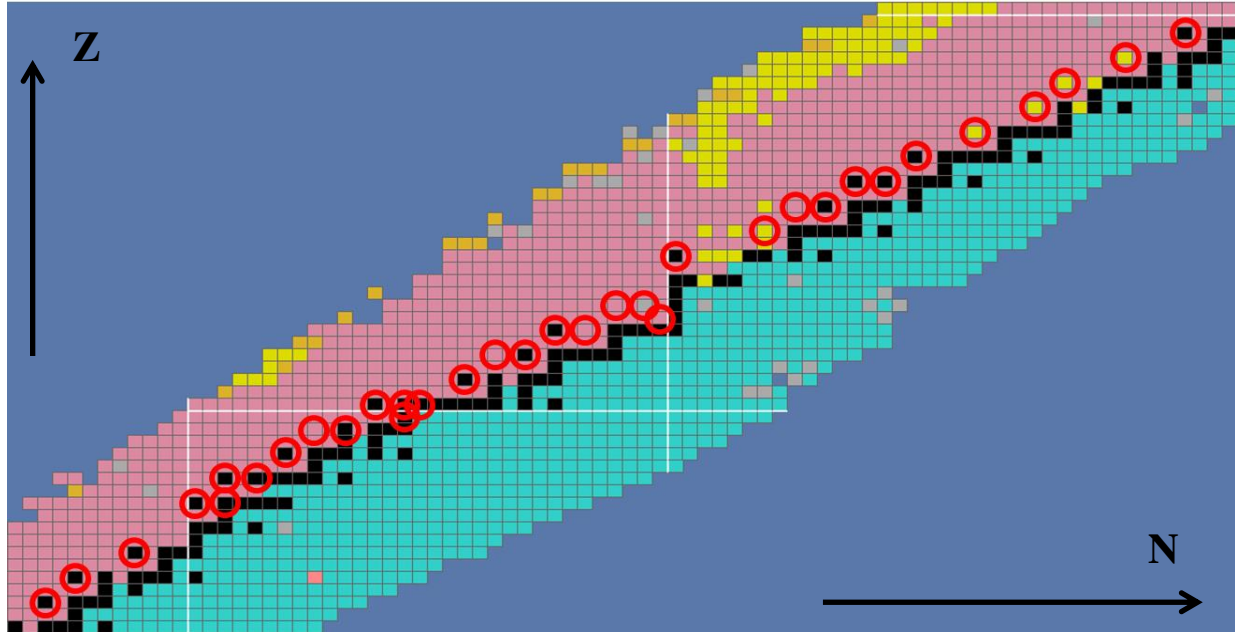


Figure 3: Chart of nuclides, with each of the 35 *p*-Nuclei encircled in red. *Z* refers to the atomic number, or number of protons in the nucleus, of an isotope, and *N* refers to the number of neutrons in the nucleus [2]. (IAEA, 2016)

The *p*-Nuclei are shielded from *r*-process decay chains by stable isotopes and are bypassed in the *s*-process reaction flow, as shown in **Figure 4** [3].

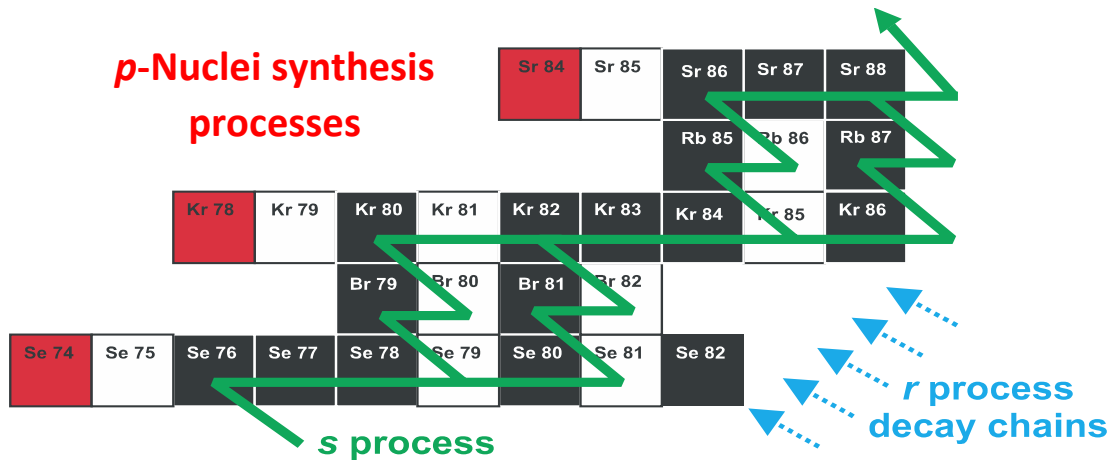


Figure 4: The rich nuclei cannot be synthesized by *s/r*-process (see text for details). (Rauscher T et al, 2013)

Typically, their solar and elemental abundances are 1 to 2 orders of magnitude less than nuclei created via neutron capture processes. These abundances are represented graphically in **Figure 5**, and quantitatively in **Table 1**.

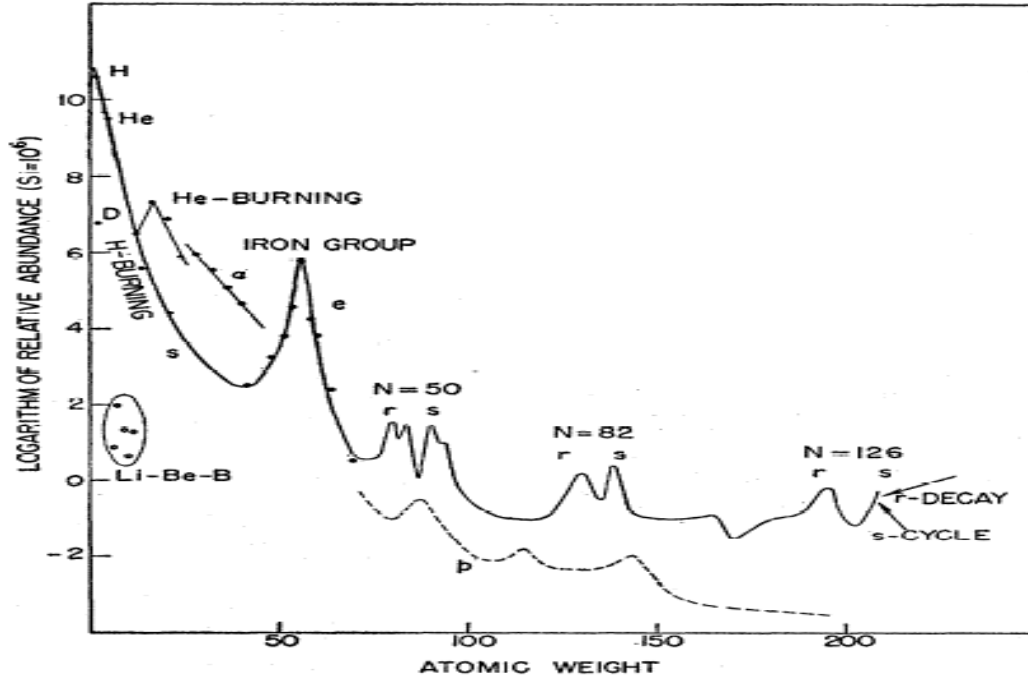


Figure 5: The abundance of elements in our solar system is shown via the solid line. The abundance of *p*-Nuclei is plotted as the dashed trendline. (Burbidge et al, 1957)

Table 1: Table of *p*-Nuclei with their relative abundances. The isotopes of molybdenum are highlighted here as the most relatively abundant *p*-Nuclei.

Isotope	% Abundance	Isotope	% Abundance	Isotope	% Abundance
⁷⁴ Se	0.87	¹¹⁴ Sn	0.66	¹⁵⁰ Dy	0.0524
⁷⁸ Kr	0.354	¹¹⁵ Sn	0.35	¹⁵⁸ Dy	0.0902
⁸⁴ Sr	0.56	¹²⁰ Te	0.089	¹⁶² Er	0.136
⁹² Mo	15.84	¹²⁴ Xe	0.126	¹⁶⁴ Er	1.56
⁹⁴ Mo	9.04	¹²⁶ Xe	0.115	¹⁶⁸ Yb	0.135
⁹⁶ Ru	5.51	¹³⁰ Ba	0.101	¹⁷⁴ Hf	0.18
⁹⁸ Ru	1.87	¹³² Ba	0.0097	^{180m} Ta	0.0123
¹⁰² Pd	0.96	¹³⁸ La	0.091	¹⁸⁰ W	0.135
¹⁰⁶ Cd	1.215	¹³⁶ Ce	0.193	¹⁸⁴ Os	0.018
¹⁰⁸ Cd	0.875	¹³⁸ Ce	0.25	¹⁹⁰ Pt	0.0127
¹¹³ In	4.28	¹⁴⁴ Sm	3.09	¹⁹⁶ Hg	0.146
¹¹² Sn	0.96	¹⁵² Gd	0.20		

Among these under-produced nuclei, the isotopes of molybdenum are the most relatively abundant, making these isotopes very appealing for investigating the origin of p -Nuclei. However, because of these low abundances, p -Nuclei are generally understudied, and astrophysical details regarding the synthesis of p -Nuclei are still in discussion [1]. While a number of potentially promising sites, such as type Ia and type II supernovae, have been theorized to produce a large portion of proton rich nuclei, current available astrophysical models cannot reproduce the solar abundances of all 35 proton rich isotopes with a single nuclear process in a given astrophysical site.

In current models, photodisintegrations (photon interaction with the emission of a particle) and β^+ decay from a neutron rich seed nucleus dominate p -Nuclei production, as demonstrated in **Figure 6** [4]. This is referred to as the γ -process. Proton absorption capture can, in principle, yield proton rich nuclei, such reaction is hindered by the electrical Coulomb potential, which increases with Z [3].

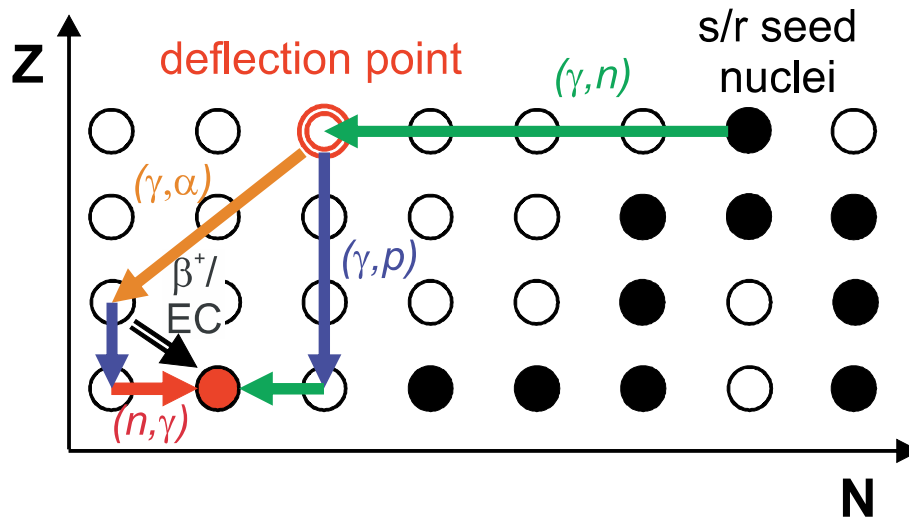


Figure 6: Reaction flow in the γ -process. (Rauscher T et al, 2013)

Despite the enduring problem of reproducing the abundances of the p -Nuclei, a recent model proposed by Travaglio *et al* achieved a remarkable breakthrough [5]. For the first time, a stellar source has been shown to produce the solar abundances of both light and heavy p -Nuclei near levels observed in our solar system. However, their results, shown in **Figure 7**, underproduce the ^{94}Mo isotope, leaving its synthesis an open question.

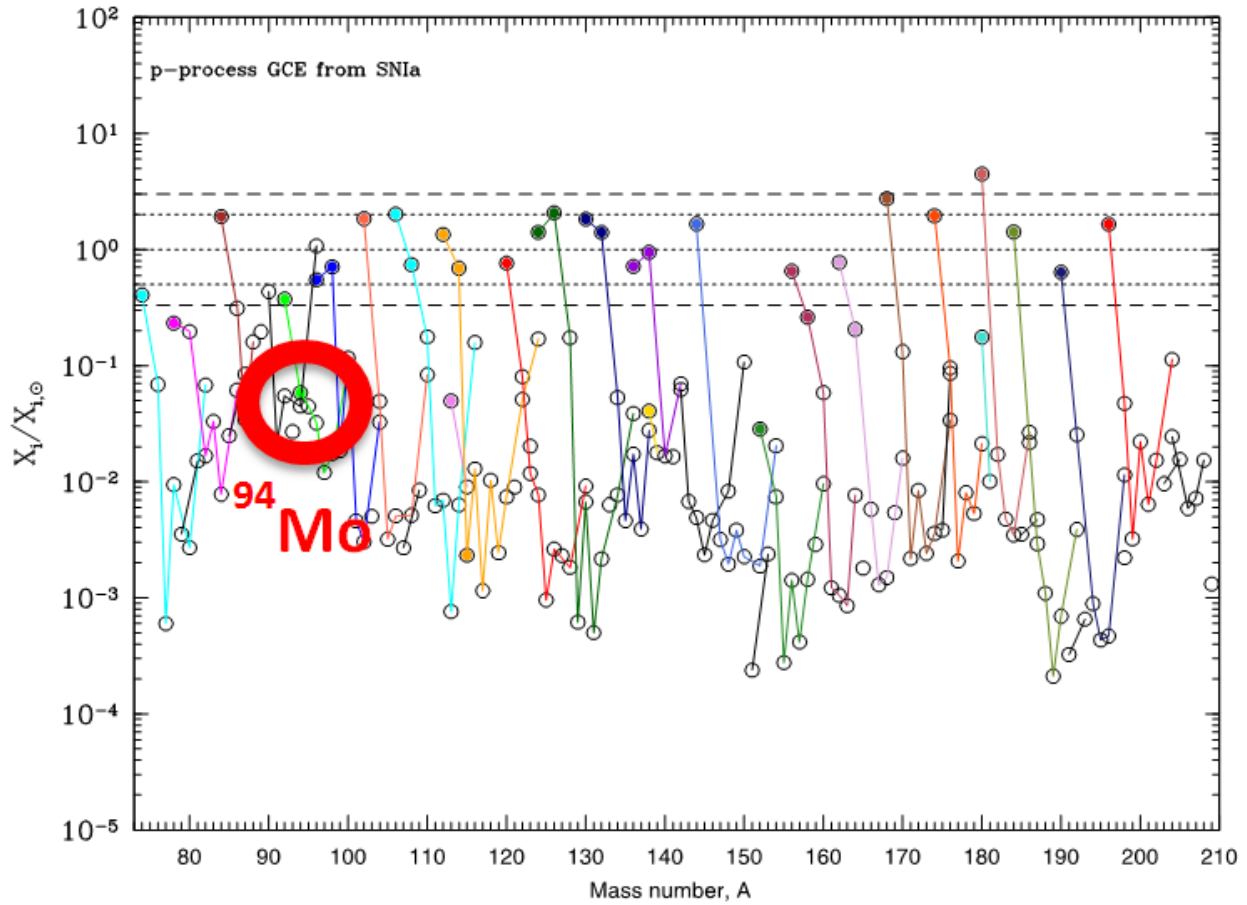


Figure 7: Isotopic abundance ratio comparing model results with observed abundances. Filled dots are for the 35 isotopes classically defined as p -only. The isotopes of each element are connected by a line, and for each element, a different color. (C. Travaglio et al, 2011)

A possible explanation for this underproduction is a lower photodisintegration probability for the ^{94}Mo isotope. Clearly, experimental determination of this cross section is warranted.

1.2 $^{94}\text{Mo}(\gamma, n)^{93}\text{Mo}$ Cross Section

When a nucleus ^AX absorbs the energy of an external photon, it will excite to higher energy levels. If the excitation energy is above the neutron/proton separation energy, that nucleus will photodisintegrate by emitting a neutron/proton, respectively. If the excitation energy is below the neutron/proton separation energy, the nucleus will scatter the incident photon, as shown in **Figure 8**.

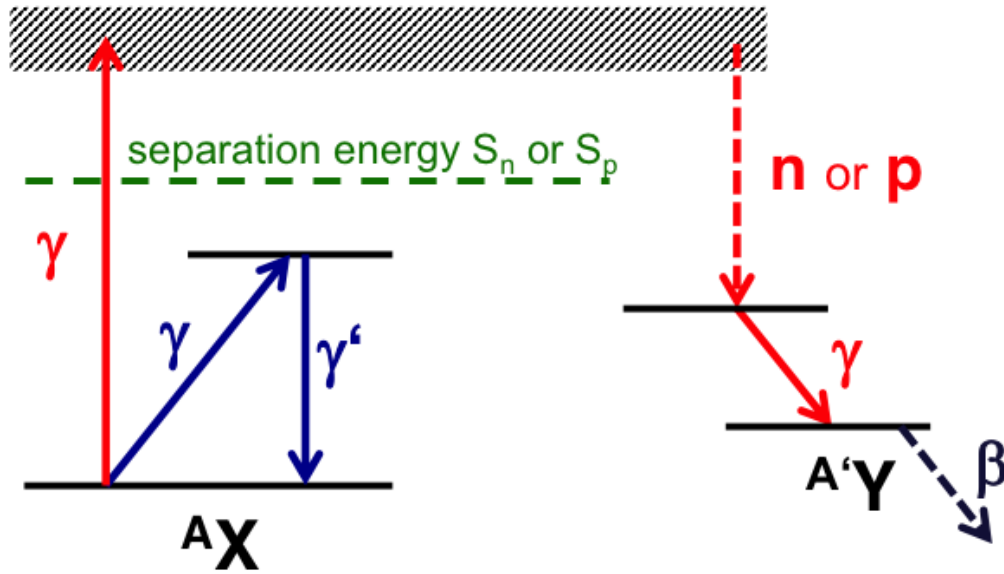


Figure 8: Simplified scheme for **photodisintegration** and **scattering** reactions on a nucleus.

In the case of the astrophysical reaction of interest here, $^{94}\text{Mo}(\gamma, n)^{93}\text{Mo}$, the neutron separation energy is 9.7 MeV[†]. Any photon beam with energy above 9.7 MeV will induce this reaction. The probability of this photodisintegration with neutron emission is referred to as the cross section of the $^{94}\text{Mo}(\gamma, n)$ reaction.

[†] 1 MeV = 10⁶ eV. An eV is defined as the energy of an electron after it is accelerated through a 1V potential difference.

Since the unstable nucleus produced by the $^{94}\text{Mo}(\gamma, n)$ reaction has a long half-life (3500 years), its nuclear decay cannot be investigated experimentally. This implies that in order to experimentally determine the cross section for the $^{94}\text{Mo}(\gamma, n)$ reaction to occur, the neutrons produced from the photodisintegration must be counted. This is given for $^{94}\text{Mo}(\gamma, n)^{93}\text{Mo}$ by the following equation:

$$\sigma(\gamma, n) = \frac{N_n}{N_\gamma N_t \epsilon_n}$$

- $\sigma(\gamma, n)$ – Cross section of the $^{94}\text{Mo}(\gamma, n)^{93}\text{Mo}$ photodisintegration reaction, and depends on the energy of the incident photon beam
- N_n – Number of neutrons emitted from the photodisintegration reaction
- ϵ_n – Efficiency of the neutron detector
- N_γ – Number of incident photons
- N_t – Number of atoms per unit area within the target [mb^{-1}]

In the spring of 2014, we successfully measured this cross section close to and above the neutron separation threshold with photon beams at the **High Intensity Gamma-Ray Source** (HIγS) facility located at Triangle University Nuclear Laboratory (TUNL). This facility was uniquely suited to carry out the experiment as a world leading source of high intensity quasi-monoenergetic γ -ray beams. The measurements were focused primarily on studying the energy dependence of the photo-neutron cross section, which is the most direct way of testing the predictions of theoretical model calculations.

Chapter 2

Experimental Method

2.1 HI γ S Facility

The HI γ S facility is currently the most intense monoenergetic photon beam source in the world, reaching intensities in excess of 10^8 photons per second. The energy of the HI γ S photon beam can range between 1-100 MeV, making the facility ideal for nuclear physics experiments. In the following section, the experimental technique used to produce the γ -ray beam at HI γ S is discussed. This technique is known as Compton back-scattering.

2.1.1 γ -Ray Beam Production at HI γ S

One way photons can interact with matter via Compton scattering, in which the incident photon gives part of its energy to an electron at rest. The photon is scattered at a lower energy and so is the electron. If the angle between the scattered photon and electron is 180° , the process is called Compton back-scattering. In the HI γ S facility, a Free Electron Laser (FEL) beam Compton back-scatters off a beam of electrons accelerated at relativistic energy to produce a high energy γ -ray beam.

In order to produce the FEL beam, electrons are released from a photocathode microwave electron gun and accelerated through a linear accelerator up to 0.28 GeV[‡]. After leaving the Linac, the electron beam is injected into the booster and is accelerated up to 1.2GeV. The

[‡] 1 GeV = 10^9 eV

electrons are sped up in the booster to relativistic speeds, and then sent into the storage ring in bunches [6].

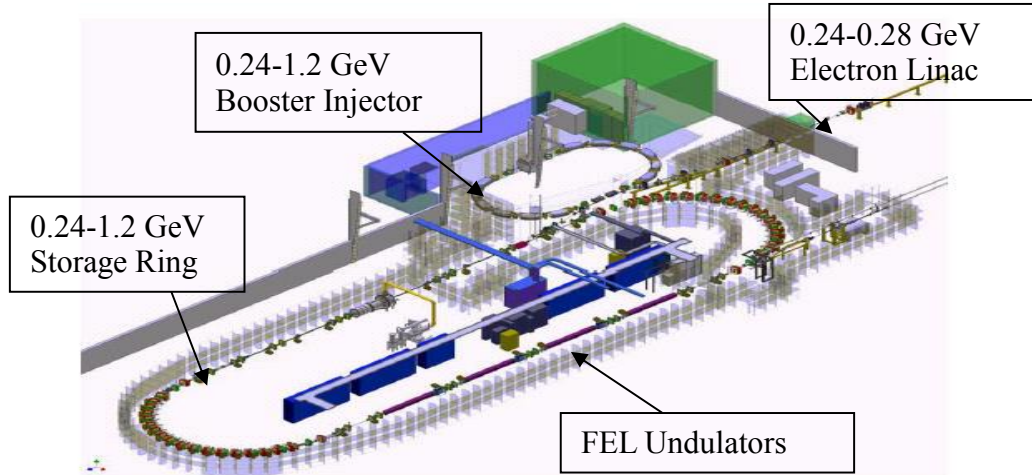


Figure 9: Layout of the HIγS facility with accelerating stages to produce the Free Electron Laser beam.

In one of the straight passages of the storage ring, the FEL laser beam is produced, as shown in **Figure 9**. The FEL photon beam, need for photon beack-scattering collision, are produced in magnetic undulators. **Figure 10** illustrates a typical magnetic undulator in which electrons transverse periodic magnetic structures, forcing the electrons to oscillate radiating photons in the forward direction of the electron beam.

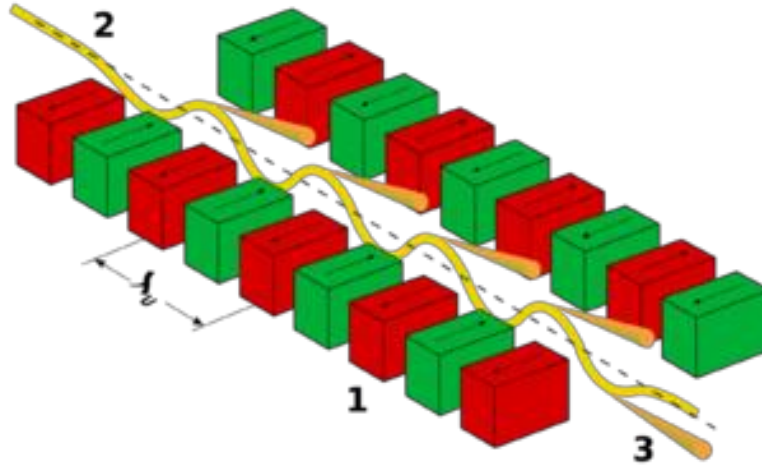


Figure 10: System of magnetic undulators, which deflect the free electron bunches to emit parallel photons.

These synchrotron radiation photons are contained in the straight passage by two optical high-reflectivity mirrors. After reflecting off the mirrors, the photons re-enter the undulator in the same direction with the next incoming electron bunch, causing an amplification in the photon bunch in a process called lasing, thus creating the FEL beam. After another reflection, the FEL beam collides with the next electron bunch head-on, causing a Compton back-scattering event. Energy is transferred from the relativistic electrons to the photons, polarizing them and increasing their energy into the MeV range. This event changes the FEL laser beam into a γ -ray beam, which can penetrate through the reflective mirror, and continue to the experimental areas. The production of the FEL beam, along with the γ -ray production, are shown schematically in **Figure 11** [7]. A simplified version of the Compton back-scattering collision between the FEL beam and the relativistic electron bunch is shown in **Figure 12**.

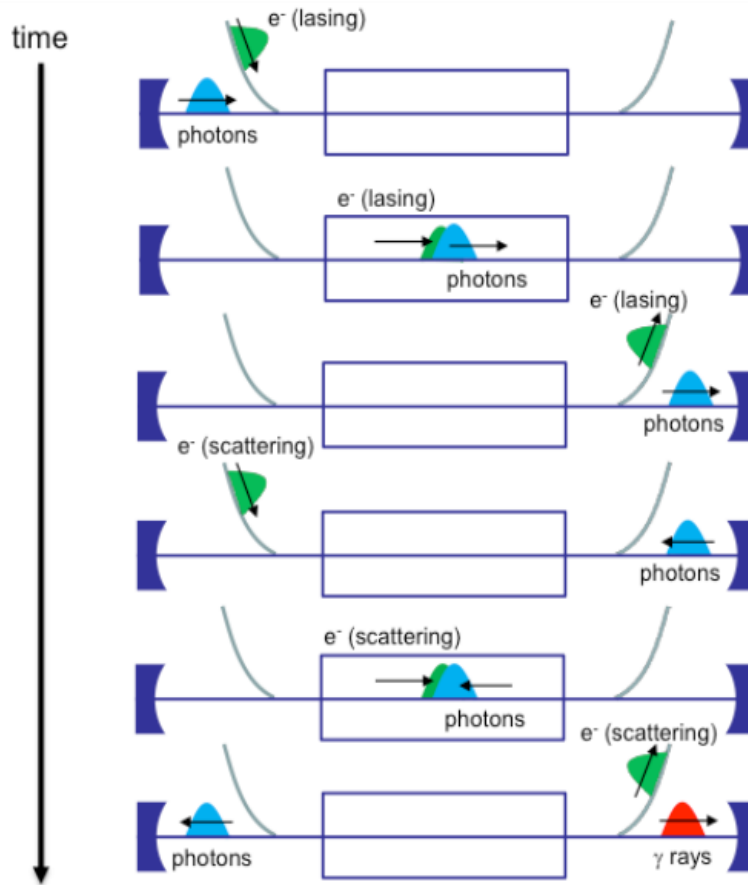


Figure 11: Free Electron Laser beam and γ -ray beam production at HI γ S (see text for details). (Carman T S et al, 1996)

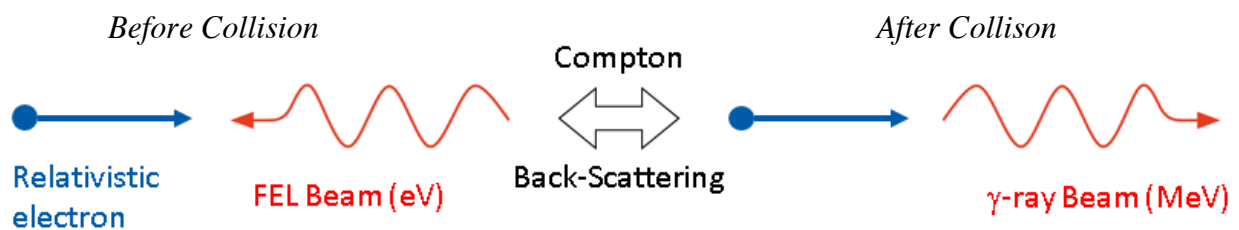


Figure 12: Simplified collision diagram of Compton back-scattering event (see text for details).

If the electrons are relativistic and the angle at which these photons are reflected backwards, θ , is small, then conservation of energy and momentum yields the following equation:

$$E_\gamma \approx \frac{4\gamma^2 \varepsilon_L}{1 + (\gamma\theta)^2 + 4\gamma\varepsilon_L / (m_e c^2)},$$

where E_γ [MeV] is the energy of the back-scattered photon, ε_L is the energy of the incident Free Electron Laser (FEL) laser beam [MeV], $\gamma = E_{\text{electron}}/m_e c^2$ is the Lorentz factor for relativistic particles, and $m_e c^2$ is the mass value of an electron, 0.511 MeV. By this method, the produced photons, initially in the keV range, increase their energy into the MeV range. By this equation, if a 3.3 eV FEL laser back-scatters off of a 450 MeV ($\gamma = 882$) electron beam, a 10 MeV γ -ray beam is produced.

2.2 Experimental Setup

In **Figure 13** is shown the experimental setup that was used at the HI γ S facility to measure the $^{94}\text{Mo}(\gamma, n)$ photodisintegration cross section of interest.

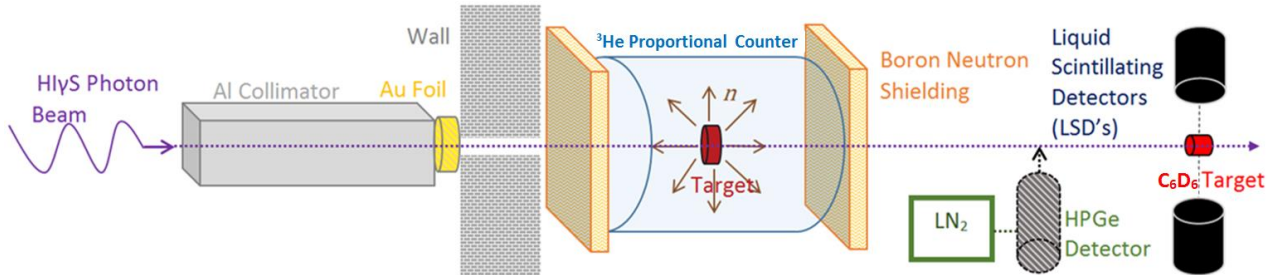


Figure 13: Experimental setup used for the photodisintegration cross section measurements.

2.2.1 Aluminum Collimator

After the HI γ S photon beam is created via Compton Backscattering, it travels through 50 meters of air before reaching the experimental area. During this travel, air particles cause many of the photons to recoil, and the beam spreads into an area larger than the ^{94}Mo target. Hence, a collimator, which was created at James Madison University, was used to tighten the beam width. While standard collimators are lead-based, their low neutron separation energy of 7.37 MeV would cause a significant source of background neutrons for all of the experimental runs. Aluminum was chosen because it has a high neutron separation energy of 13.06 MeV, and thus would not be a source of neutron emission background for over half of photon beam energies used in this experiment, including those deemed most important to our study.

Since the target disk is 2 centimeters in diameter, the photon beam was collimated to a diameter of 1.5 centimeters. This not only meant that the aluminum collimator would need to have a 1.5 cm diameter bore through it, but also that it be long enough to attenuate all stray photons out of the beam. Based on this geometry and the energy range of this experiment (9.7-18 MeV), a collimator length of approximately 1 meter was chosen. This produced a very tight beam with a size smaller than that of the target used, as seen in **Figure 14**.

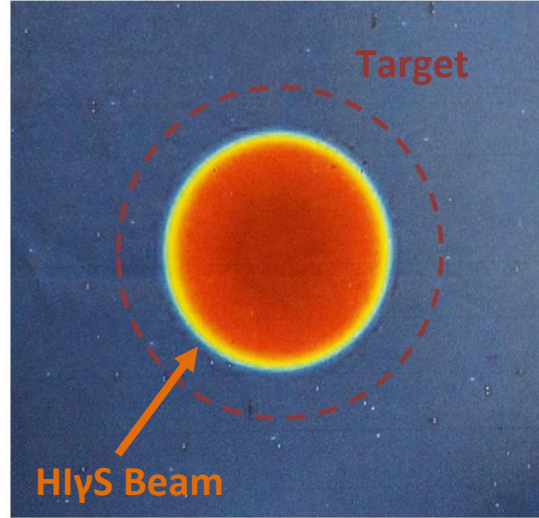


Figure 14: HI γ S photon beam image on target after collimation. The image shows that the HI γ S beam is well focused within the target area (dashed circle).

2.2.2 ^3He Proportional Counter Array

[Put proposal line here, explaining interaction] The neutron ^3He proportional counter array contains two rings of nine ^3He tubes, each 39.4 cm in length and equally spaced from each other. The inner ring is a distance of 7.24 cm from the axial cavity, and the outer ring a distance of 10.60 cm. The ^3He tubes are embedded in a cylindrical polyethylene body 46.2 cm long and 30.5 cm in diameter. This geometry is shown in **Figure 15**.

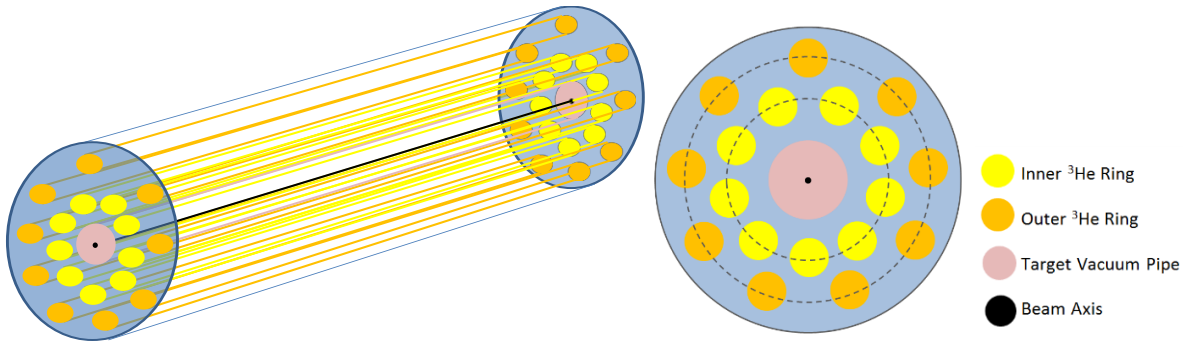


Figure 15: The ^3He proportional counter array detector used in this experiment. The ^3He proportional counter array is cylindrical with two sets of nine tubes of ^3He , arranged symmetrically around the beam axis. The material between the helium tubes is paraffin.

The axial cavity has a diameter of 8.9 cm. After a neutron is emitted from the $^{94}\text{Mo}(\gamma, n)$ photodisintegration reaction, it has a probability to impinge upon the ^3He nuclei and interact with the counter array. Upon activation, the proportional counter generates logic output signals corresponding to the detection (or lack thereof) of a neutron. The paraffin body of the ^3He proportional counter array is designed to thermalize impinging neutrons, increasing the probability of the neutron interaction and thus electronic signal output. This detector has an efficiency of ~50-60%, depending on the energy of the neutrons emitted from the target. The electronics connected to the ^3He proportional counter array detector was set up to allow for both offline storage of data as well as live measurements of the neutron intensity [8]. In this experiment, this setup was operated in vacuum to reduce background from photon interaction with nuclei in the air, such as the $^{14}\text{N}(\gamma, n)$ reaction.

2.2.3 HPGe Detector

Before each experimental run, a HPGe detector was used to measure the energy peak of the $\text{HI}\gamma\text{S}$ photon beam. The HPGe was swung in line of the photon beam by a mechanical arm every time it was used, allowing the device to maintain a constant geometry throughout the experiment.

2.2.4 Flux Determination Equipment

The gold foil placed at the end of the collimator, as well as the heavy benzene/liquid scintillator system further downstream, were utilized to determine the photon beam flux for the experimental runs. This is the focus of my thesis, and will be discussed in detail in the following section.

Section 3

HI γ S Photon Beam Intensity Determination

To determine the rate of incident photons in the produced HI γ S beam, two different methods were used. For 11 photon energies, ^{197}Au foils were placed one at a time at the entrance of the aluminum collimator along the axis of the photon beam, as seen in **Figure 13**. γ -rays de-exciting the radioactive ^{196}Au nucleus, produced via $^{197}\text{Au}(\gamma, n)$ photodisintegration reaction, were counted offline. This is known as photoactivation method and was used to measure the beam intensity for the experimental runs at the following HI γ S beam energies: 9.6 MeV, 9.7 MeV, 9.8 MeV, 9.9 MeV, 10.0 MeV, 11.85 MeV, 11.95 MeV, 12.05 MeV, 12.15 MeV, 12.25 MeV, and 14.0 MeV. The HI γ S photon beam intensity was measured for every experimental run using a $^2\text{H}(\gamma, n)$ photodisintegration reaction.

While both methods were implemented to determine the photon beam intensity throughout the experiment, this thesis will focus on the efforts and results involving the photoactivation method. The full analysis of the $^2\text{H}(\gamma, n)$ monitor reaction data will be complete in the near future. Here, only an overview of the data analysis regarding the $^2\text{H}(\gamma, n)$ reaction will be discussed.

3.1 Photoactivation Method

Before each experimental run corresponding to ^{197}Au photoactivation, a gold foil was precisely taped onto the end of the aluminum collimator so that the center of the foil aligned with the center of the collimator bore, as shown in **Figure 13**. Since the area of the gold foil was slightly larger than that of the collimator bore, the gold foil saw the same photon flux as the ^{94}Mo target. The times at which the photoactivation started and when it was complete were recorded very accurately.

There were three distinct advantages for which the photoactivation of ^{197}Au isotope as monitor reaction was specifically chosen. Firstly, the cross section of the $^{197}\text{Au}(\gamma, n)$ reaction, shown in **Figure 16** for a broad range of photon energies, is very well understood from previous studies. Secondly, this reaction has one of the highest (γ, n) cross sections, thus reducing activation time greatly. Thirdly, the half-life and decay energy of the excited daughter nucleus are very convenient for offline measurements, as discussed later on in this section [9].

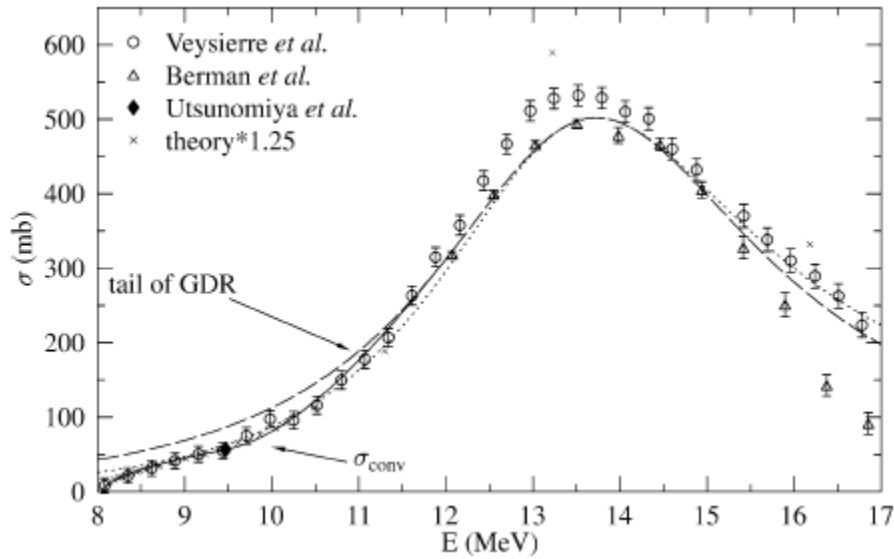


Figure 16: Energy dependence of $^{197}\text{Au}(\gamma, n)$ cross section reaction. (K. Vogt et al, 2002)

After irradiation, a low-background 60% HPGe detector, combined with a Canberra Multiport II multichannel analyzer, was used to count the activity of the gold foil monitor offline. There were four HPGe detectors available for offline measurement located in a low-background vault.

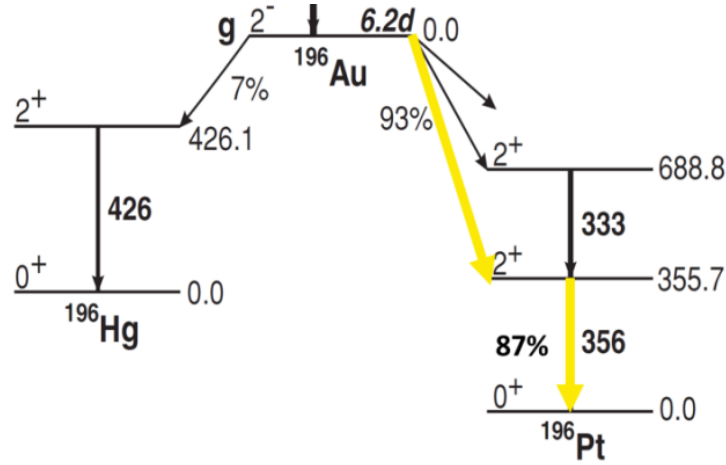


Figure 17: Decay scheme of the ^{196}Au isotope. All energies are given in keV. (A. Tsinganis et al, 2011)

As shown in **Figure 17**, the unstable ^{196}Au has a half-life of 6.2 days and decays through two primary pathways. The pathway on the left hand side has a 7% probability and β^- -decays to ^{196}Hg isotope, while the pathway on the right hand side has a 93% probability and decays via electron capture to ^{196}Pt isotope. We chose the dominant pathway to evaluate the HI γ S beam intensity. With a 87% relative intensity, the 356 keV γ -ray transition between the first excited state and the ground state of ^{196}Pt was the focus of detection with the HPGe detector for offline counting. The photon intensity was determined by using the activation equation:

$$\Phi_{\gamma} = \frac{N_{356} \lambda_{196}}{\sigma(\gamma, n) N_{197} i_{356} T \epsilon_{356}}$$

- Φ_{γ} – Intensity of the HI γ S beam in photons per second [pps]
- N_{356} – Number of detected γ -rays in the 356 keV photopeak
- λ_{196} – Decay constant for ^{196}Au (1.3×10^{-6} Hz) [s^{-1}] [10]
- $\sigma(\gamma, n)$ – Cross section of $^{197}\text{Au}(\gamma, n)$ [mb]
- N_{197} – Number of ^{197}Au atoms per unit area in the foil [mb^{-1}]
- i_{356} – Relative intensity of the 356 keV γ -ray transition multiplied by the electron capture probability, yielding a value of 80% [11]
- T – Time correction factor
- ϵ_{356} – Photopeak efficiency of the HPGe detector

Each of these factors were determined as follows.

N_{356} is calculated through analysis of the γ -ray spectrum using the TV γ -ray spectroscopy software package [12]. A typical γ -ray spectrum of the HPGe detector produced by a multichannel analyzer is uncalibrated (γ -ray energies are expressed in channels of the multichannel analyzer). An energy calibration was warranted. This was done by finding a linear relationship between two known photopeak energies and their channel equivalents. A calibration is detector-specific, so four different calibrations were used in this experiment, one for each HPGe detector.

When determining the count number in the 356 keV photon peak area, two different methods were implemented, each with their advantages and disadvantages that depended on the peak shape and γ -ray background. The first method utilized a simple peak summation that removes background hits from the summation. While robust, this method only works if the 356 keV photopeak does not overlap with any other photopeak, namely the 333 keV energy, which corresponds to another dominant γ -ray transition in the decay of ^{196}Au (see **Figure 17**).

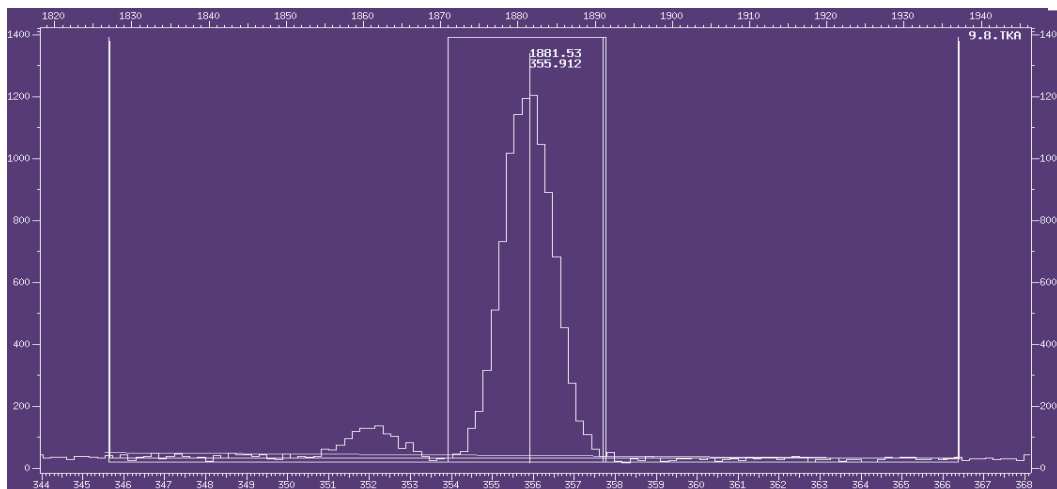


Figure 18: Energy spectrum (counts vs energy) taken with a multichannel analyzer showing the 356 keV photopeak, as produced with the TV software (see text for details) using the peak summation method.

If the two peaks overlap, the TV software was used for a second analysis method, the Gaussian fit. This method overlays separate Gaussian curves on each photopeak. Like the peak summation method, the Gaussian fit accounts for background, and delivers an accurate peak summation.

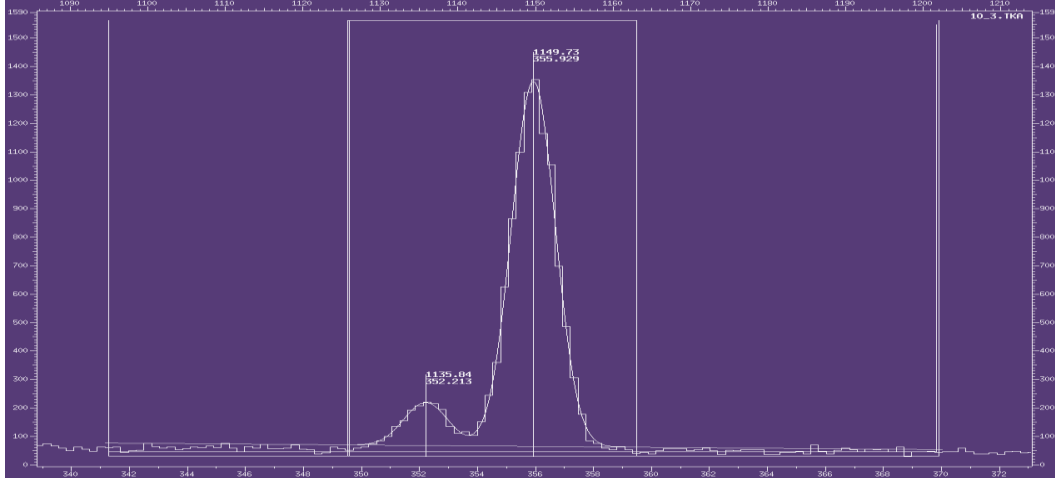


Figure 19: The analysis of the 356 keV photon using the Gaussian fit method

While the Gaussian fit function seems to give more accurate results, it yields a slightly larger error than the peak summation. While this error is not significant, the peak summation method was used whenever appropriate [12]. The energy dependence of $\sigma(\gamma, n)$ is illustrated in **Figure 16**, and approximated using the formulas in **Table 2** [9].

Table 2: Recommended parameterization of the $^{197}\text{Au}(\gamma, n)$ cross section. E_{THR} (8.071 MeV) is the neutron separation energy for $^{197}\text{Au}(\gamma, n)$. (K. Vogt et al, 2002)

Energy region (MeV)	Formula	Uncertainty (%)	Parameters
8.071–9.5	$\sigma_0 \cdot [(E - E_{\text{thr}})/E_{\text{thr}}]^p$	6	$\sigma_0 = 146.2 \text{ mb}$ $p = 0.545$
9.5–12	$a_1 + a_2 E + a_3 E^2 + a_4 E^3$	6–2	$a_1 = 7399.31 \text{ mb}$ $a_2 = -1988.29 \text{ mb/MeV}$ $a_3 = 171.493 \text{ mb/MeV}^2$ $a_4 = -4.58479 \text{ mb/MeV}^3$
12–14.714	$\sigma_m \cdot \frac{(\Gamma E)^2}{(E^2 - E_{\text{GDR}}^2)^2 + (\Gamma E)^2}$	2	$\sigma_m = 502 \text{ mb}$ $\Gamma = 4.76 \text{ MeV}$ $E_{\text{GDR}} = 13.73 \text{ MeV}$

Figure 20 shows the time-line of the photoactivation process, which begins with the irradiation of ^{197}Au and ends with the offline counting of the decay of ^{196}Au .

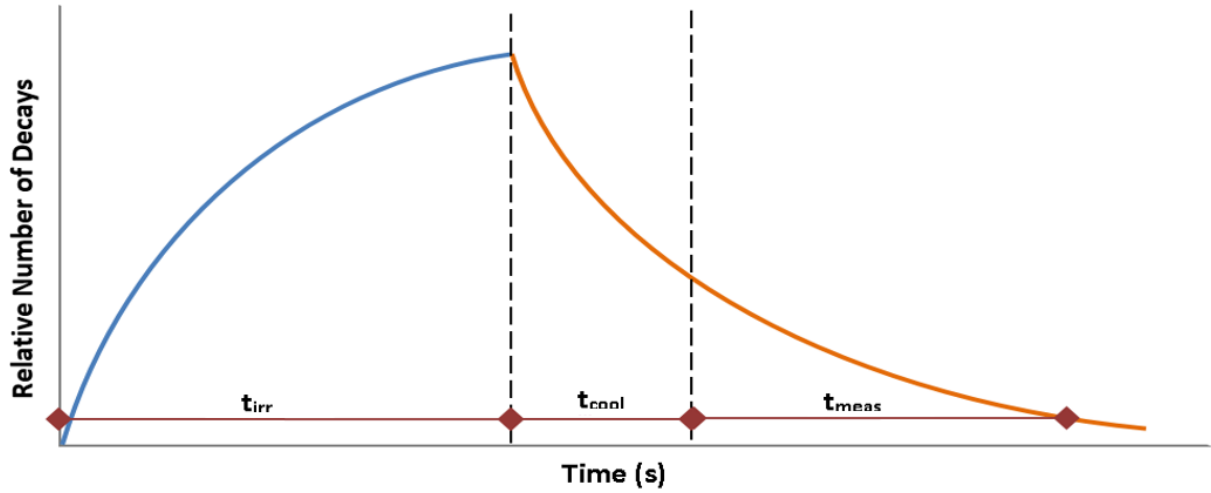


Figure 20: The blue line represents the period of activation for ^{197}Au , t_{irr} . The orange line represents the period after activation, broken up into a cooling period, t_{cool} , and the time for HPGe measurement, t_{meas} .

The time correction factor T was calculated using the following equation:

$$T = (1 - e^{-\lambda_{196} t_{\text{irr}}})(e^{-\lambda_{196} t_{\text{cool}}})(1 - e^{-\lambda_{196} t_{\text{meas}}})$$

where t_{irr} is the irradiation time of ^{197}Au , t_{cool} is elapsed cooldown time between irradiation and offline counting, and t_{meas} is the offline counting time, all in seconds.

ϵ_{356} is the detection efficiency of 356 keV γ -ray by a HPGe detector. It was determined for each of the four HPGe detectors. A mixed source of radioisotopes was employed for efficiency calibration. A typical γ -ray spectrum of the mixed source is shown in **Figure 21**, as it was generated with the TV software.

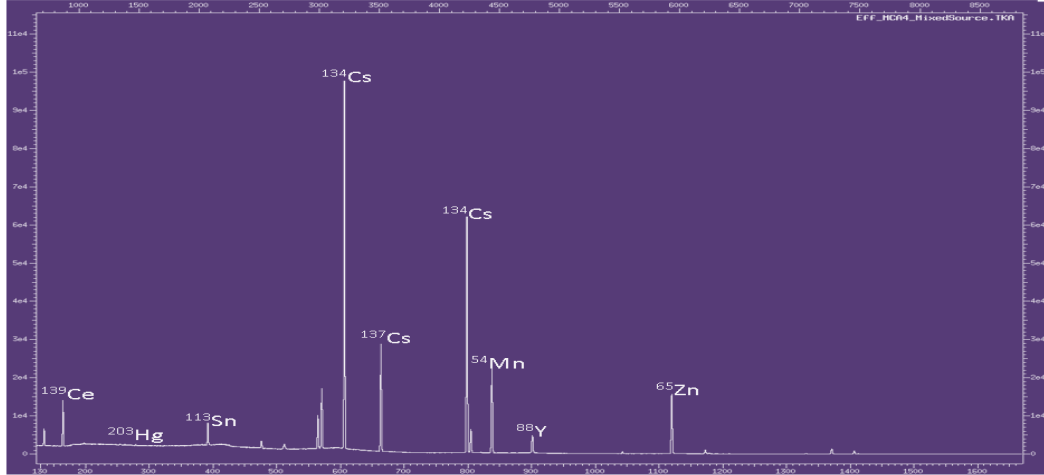


Figure 21: Mixed source γ -ray energy spectrum produced by the TV software. The figure shows the more intense γ -ray transitions in the isotopes present in the mixed source used in the experiment.

In **Table 3** are presented the characteristics of the radioisotopes in the mixed source.

Table 3: Radioisotopes from the mixed source used in HPGe detector efficiency calibration

Isotope	γ Emission Energy (keV)	Original Activity (Bq)	Half-Life (days)	Activity (Bq)
^{241}Am	59.5	2.398E+03	1.580E+05	2.393E+03
^{109}Cd	88.0	2.145E+03	4.626E+02	1.070E+03
^{57}Co	122.1	1.319E+03	2.718E+02	4.041E+02
^{139}Ce	165.9	1.677E+03	1.376E+02	1.620E+02
^{203}Hg	279.2	4.096E+03	4.661E+01	4.133E+00
^{113}Sn	391.7	2.704E+03	1.151E+02	1.655E+02
^{134}Cs	604.7	7.229E+03	7.542E+02	4.720E+03
^{137}Cs	661.7	1.502E+03	1.098E+04	1.459E+03
^{134}Cs	795.9	6.329E+03	7.542E+02	4.132E+03
^{54}Mn	834.9	4.173E+03	3.121E+02	1.489E+03
^{88}Y	898.0	7.237E+03	1.066E+02	3.544E+02
^{65}Zn	1115.6	5.614E+03	2.441E+02	1.504E+03
^{88}Y	1836.1	7.662E+03	1.066E+02	3.753E+02

The efficiency of the HPGe detector was calculated as the ratio between the detected activity (counts per second) and the corresponding real activity of each of γ -rays shown in **Table 3**. Using PsiPlot [psipLOT], the following function was then fit to the data points.

$$eff(E) = e^{A+B*\ln(E)+C*(\ln(E))^2}$$

with , B , and C as fit parameters determined by PsiPlot. In **Figure 22**, we present the efficiency calibration plots for each of the four HPGe detectors used for offline counting.

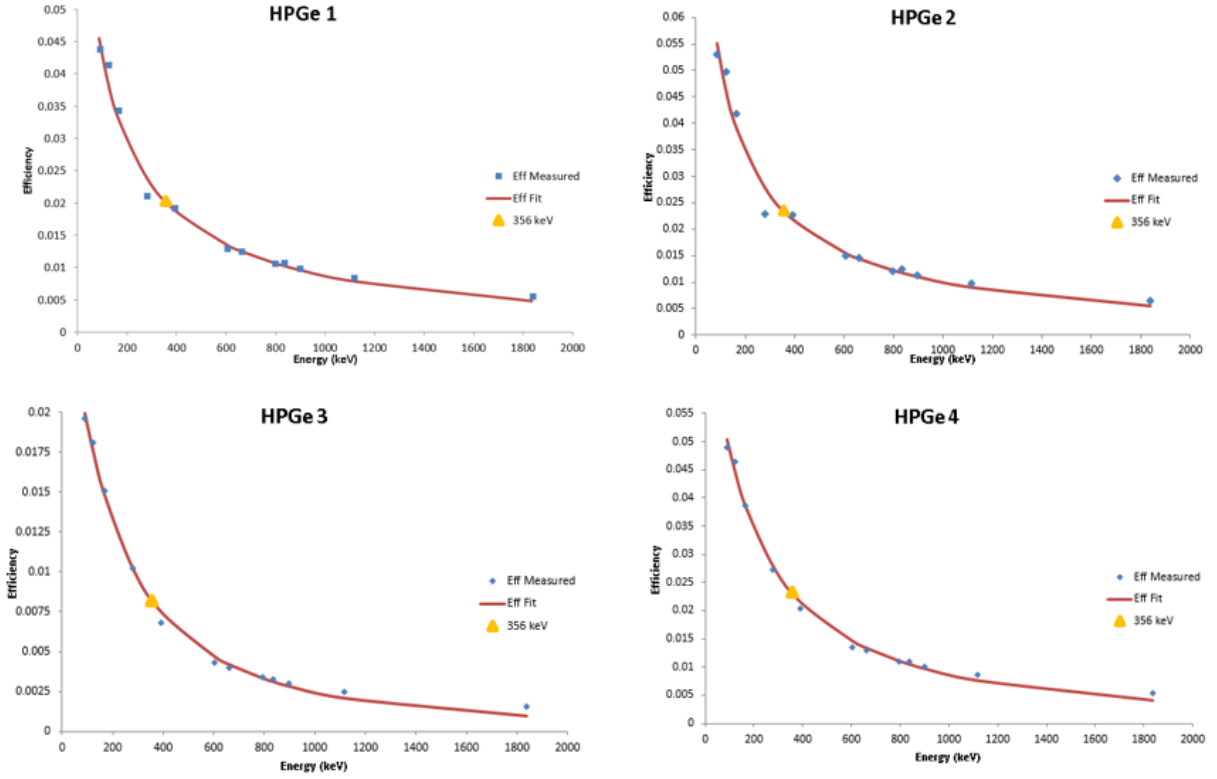


Figure 22: The efficiency of each energy detected from the standardized mixed source for each of the four HPGe detectors. A fit based on the parameters described in the text is marked in red, and the location of the 356 keV photon efficiency is shown in yellow.

The results from all four HPGe efficiency plots are listed in **Table 4**.

Table 4: HPGe efficiency result table

HPGe Detector	Efficiency for 356 keV	Efficiency Error
#1	0.020	$\pm 0.98\%$
#2	0.024	$\pm 0.90\%$
#3	0.0078	$\pm 0.82\%$
#4	0.02268	$\pm 2.3\%$

3.1.1 Photon Beam Intensity Results

By utilizing the aforementioned activation equation, **Table 5** as well as **Figure 23**, present the results of the HI γ S photon beam intensity (photons per second).

Table 5: Photon beam determination results using the photoactivation method

Beam E (MeV)	Gold Foil #	$\sigma(\gamma, n)$ (mb)	ϵ_{356}	Φ_γ (pps)
9.6	6	60.19	0.02357	8.735E7
9.7	4	64.26	0.02031	9.196E7
9.8	5	69.08	0.02257	8.973E7
9.9	7	74.65	0.00778	8.809E7
10.0	8	80.92	0.02357	9.223E7
11.85	2	290.4	0.02031	1.218E8
11.95	1	305.0	0.02257	1.158E8
12.05	3	319.7	0.00778	1.180E8
12.15	9	334.7	0.02257	1.186E8
12.25	10	349.9	0.00778	1.206E8
14	11	495.7	0.02357	1.618E8

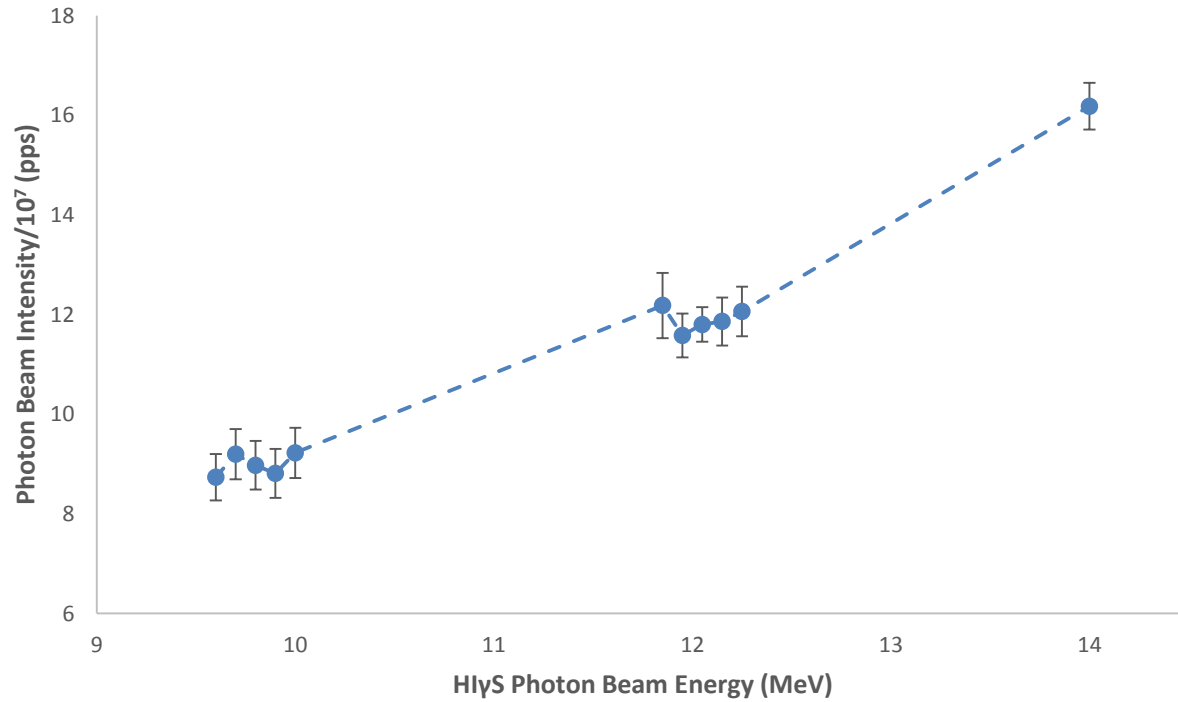


Figure 23: Results of photon beam intensity plotted against beam energy for each run the photoactivation method was used.

3.1.2 Error Analysis

As per error propagation formalism, when evaluating the error in a physical experiment, the error on a function $y(x_1, x_2, \dots)$ is written as:

$$\Delta y = y \sqrt{\left(\frac{\delta y}{\delta x_1}\right)^2 + \left(\frac{\delta y}{\delta x_2}\right)^2 + \dots}$$

In the case where all x factors of the y function are neither inside of a separate function or raised to a power besides ± 1 , then the equation can be simplified to:

$$\Delta y = y \sqrt{\left(\frac{\Delta x_1}{x_1}\right)^2 + \left(\frac{\Delta x_2}{x_2}\right)^2 + \dots}$$

Analyzing the aforementioned activation equation, we can derive the following uncertainty for of the photon beam intensity:

$$\Delta \Phi_\gamma = \Phi_\gamma \sqrt{\left(\frac{\Delta N_{356}}{N_{356}}\right)^2 + \left(\frac{\Delta \lambda_{356}}{\lambda_{356}}\right)^2 + \left(\frac{\Delta \sigma(\gamma, n)}{\sigma(\gamma, n)}\right)^2 + \left(\frac{\Delta N_{197}}{N_{197}}\right)^2 + \left(\frac{\Delta i_{356}}{i_{356}}\right)^2 + \left(\frac{\Delta \epsilon_{356}}{\epsilon_{356}}\right)^2 + \left(\frac{\Delta T}{T}\right)^2}$$

ΔN_{356} was evaluated in the TV program by convoluting Poisson distribution uncertainties, characteristic to a radioactive decay, and the Gaussian fit error.

$\Delta \lambda_{196}$ has been taken from literature to be 0.01%, and was considered negligible [10].

$\Delta \sigma(\gamma, n)$ has been thoroughly studied previously, as quantified in **Table 2**.

ΔN_{197} was determined from the errors associated with the equipment used to measure the mass and diameter of the ^{197}Au foils, as well as the diameter of the aluminum collimator. Since

these measurements were performed with high-precision equipment, ΔN_{197} is considered negligible in solving for $\Delta \Phi_\gamma$.

i_{356} is written as:

$$i_{356} = i_{Pt} i_{356keV},$$

where i_{Pt} is the probability of the decay pathway to ^{196}Pt , and i_{356keV} is the relative intensity of the 356 keV photon in this decay branch. Δi_{356} is written as:

$$\Delta i_{356} = i_{356} \sqrt{\left(\frac{\Delta i_{Pt}}{i_{Pt}}\right)^2 + \left(\frac{\Delta i_{356keV}}{i_{356keV}}\right)^2}$$

It has been studied previously that $i_{356} = 0.8091$, $\Delta i_{Pt} = 0.003$, $i_{Pt} = 0.93$, $\Delta i_{356keV} = 0.03$, and $i_{356keV} = 0.87$ [10]. Thus:

$$\Delta i_{356} = 0.028$$

$\Delta \epsilon_{356}$ was calculated for each of the HPGe detectors used for offline counting. The two taken into account were the error of the efficiency fit for the mixed source data and the error on the efficiency value for 356 keV γ -ray. The corresponding results are presented in **Table 6**.

Table 6: Relative efficiency of the 356 keV photopeak corresponding to each of the four detectors used in offline counting.

HPGe	$\Delta \epsilon_{356}/\epsilon_{356}$
#1	0.0098
#2	0.0090
#3	0.0079
#4	0.0064

Since the timing in the experiment had a confidence of seconds, as compared to irradiation time intervals of at least half an hour, ΔT is negligible.

3.2 Deuterium Photodisintegration Method

Photon beam intensity was primarily determined by measuring the ${}^2\text{H}(\gamma, n)$ photodisintegration in a deuterated benzene (C_6D_6) sample. This method was chosen as the primary method for measuring the HI γ S beam intensity due to its two significant advantages over the photoactivation method. Firstly, the ${}^2\text{H}(\gamma, n)$ cross section, shown in **Figure 24**, has been studied extensively and yields an uncertainty of $\pm 5\%$, as compared to the $\pm 10\%$ uncertainty of the ${}^{197}\text{Au}(\gamma, n)$ cross section [9,13]. Secondly, the logistics for measuring the ${}^2\text{H}(\gamma, n)$ photodisintegration did not limit how often the method could be implemented, whereas each ${}^{197}\text{Au}$ foil required a HPGe detector for a substantial period of time in the photoactivation method. [14]

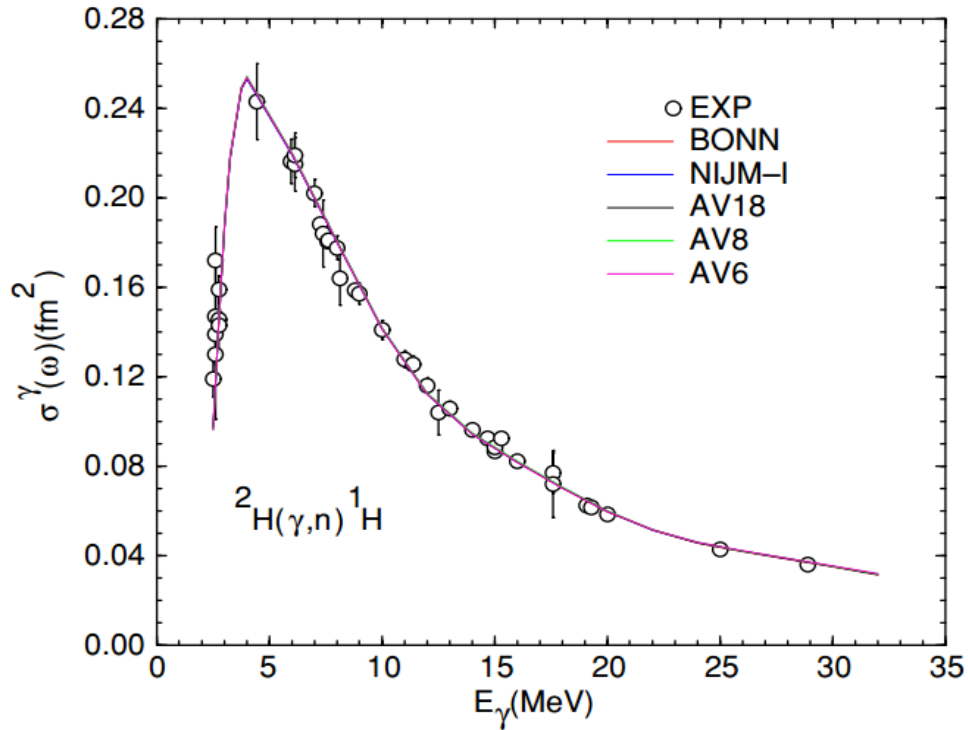


Figure 24: Deuteron photodisintegration cross section dependence beam energy. (R. Schiavilla, 2005)

The HI γ S photon beam intensity is determined by using the $^2\text{H}(\gamma,n)$ photodisintegration equation below:

$$\Phi_{\gamma} = \frac{N_n}{t \sigma(\gamma, n) N_D \epsilon_n},$$

where t is the time of the experimental run, N_n is the number of neutrons detected, $\sigma(\gamma, n)$ is the cross section for the deuterium photodisintegration reaction, seen in **Figure 24**, N_D is the number of deuterium atoms per unit area in the benzene target, and ϵ_n is the neutron detection efficiency, determined from GEANT4 Monte Carlo simulations [15].

As seen in **Figure 25**, two liquid scintillator detectors were placed lateral to the deuterated benzene sample. Liquid scintillators were chosen because of their ability to differentiate various sources of background. Along with sources of environmental background, the HI γ S photon beam scatters in the benzene, creating a large source of high energy background photons. Current data analysis is focusing on cutting out these background signals through constant fraction discrimination, time of flight evaluation, and pulse shape discrimination.

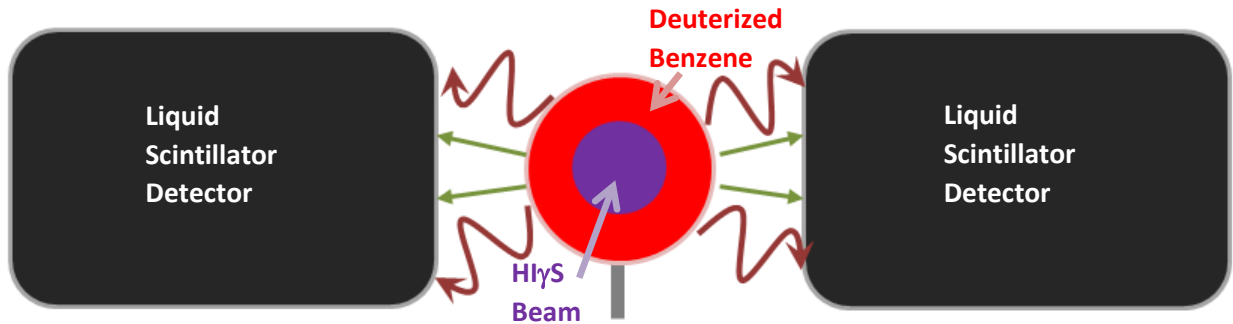


Figure 25: Setup of liquid scintillator detectors flanking the deuterated benzene sample, along with the **neutrons** and **photons** emitted from the $^2\text{H}(\gamma,n)$ photodisintegration.

While the $^2\text{H}(\gamma, n)$ monitor reaction was the more advantageous of the two intensity determination methods, its results needed to be validated by photoactivation method results to ensure accuracy. Preliminary data analysis shows agreement between the two methods.

Chapter 4

Outlook

The photon beam intensity is a key parameter in the determination of the $^{94}\text{Mo}(\gamma, n)^{93}\text{Mo}$ photodisintegration cross section (see **Section 1.2**). The photoactivation method, which is the core of this thesis work, is the only way to validate the accuracy of the photon beam intensity determined via the $^2\text{H}(\gamma, n)$ photodisintegration method for every photon beam energy. Once the neutron detection efficiency in the ^3He proportional counters is accounted for from GEANT4 Monte Carlo simulations, the cross section for the $^{94}\text{Mo}(\gamma, n)^{93}\text{Mo}$ photodisintegration reaction will be determined for the energy range starting at 9.5 MeV up to 18.5 MeV [15]. These results will be compared to the theoretical predictions as nuclear physics input for astrophysical models to more accurately predict the abundances of *p*-Nuclei in our solar system.

References

- [1] E. M. Burbidge, G. R. Burbidge, W. A. Fowler, & F. Hoyle 1957 Synthesis of the Elements in Stars *Rev. Mod. Phys.* **29(4)**, 547
- [2] Nuclear Data Services. *Livechart – Table of Nuclides*. International Atomic Energy Agency, 2016. Accessed 4/1/2016.
- [3] Rauscher T et al 2013 Constraining the astrophysical origin of p-nuclei through nuclear physics and meteoritic data *Rep. Prog. Phys.* **76(6)**, 066201
- [4] K. S. Krane *Introductory Nuclear Physics, 3rd edition* Charlottesville, VA: John Wiley & Sons, 1988, 272
- [5] Travaglio C et al 2011 Type 1a Supernovae as Sites of the p-process: Two-dimensional Models Coupled to Nucleosynthesis *Ap. J.* **739(2)**, 93
- [6] Weller H R et al 2003 The HIγS Facility: A Free-Electron Laser Generated Gamma-Ray Beam for Research in Nuclear Physics *Modern Phys. Lett. A* **18(23)**, 1569-1590
- [7] Carman T S et al 1996 The TUNL-FELL inverse Compton γ -ray source as a nuclear physics facility *Nucl. Instr. And Meth. A* **378(1)**, 1-20
- [8] Arnold C W et al 2011 Characterization of an INVS model IV neutron counter for high precision (γ, n) cross-section measurements *Nucl. Instrum. Methods in Physics Research A* **647**, 55
- [9] Vogt K et al 2002 Measurement of the (γ, n) cross section of the nucleus ^{197}Au close above the reaction threshold *Nucl. Phys. A* **707(1-2)**, 241-252
- [10] Xiaolong H 2007 Nuclear Data Sheets **108**, 1093

- [11] Tsinganis A et al 2011 Isomeric cross section of the $^{197}\text{Au}(n,2n)$ reaction *Phys. Rev. C* **83(3)**, 535-539
- [12] Schulze R 2007 Parse::TV Institute for Nuclear Physics, University of Cologne, Germany
- [13] Schiavilla R 2005 Induced polarization in the $^2\text{H}(\gamma,\vec{n})^1\text{H}$ reaction at low energy *Phys. Rev. C* **72(3)**, 034001
- [14] Perdue B A et al 2011 Cross section for three-body photodisintegration of ^3He at $E_\gamma = 12.8$, 13.5, and 14.7 MeV. *Phys. Rev. C* **83**, 034003
- [15] S. Agostinelli et al 2003 Geant4: a simulation toolkit *NIM A* **506(3)**, 250-303